

Tailored One- and Two-Dimensional Self-Assembly of a Perylene Diimide Derivative in Organic Solvents

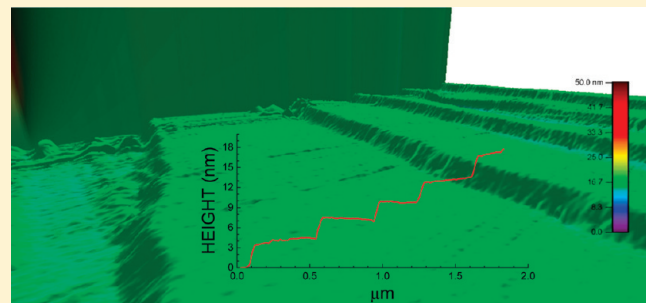
Michał T. Usowicz,[†] Michael J. Kelley,[†] Kenneth D. Singer,[†] and Volodimir V. Duzhko^{*,†,‡}

[†]Department of Physics, Case Western Reserve University, Cleveland, Ohio 44106, United States

[‡]Department of Polymer Science and Engineering, University of Massachusetts, Amherst, Massachusetts 01003, United States

 Supporting Information

ABSTRACT: We report on studies of the tailored self-assembly of the perylene diimide derivative, *N,N'*-ditridecylperylene-3,4,9,10-tetracarboxylic diimide, into structures with fibrous gel-type, one-dimensional, and two-dimensional morphologies. This approach for producing highly ordered nanostructures of well-defined morphologies utilizes a property of π -conjugated molecules to assemble in poor organic solvents due to $\pi-\pi$ interaction between the aromatic cores and takes advantage of the temperature dependence of solubility. The morphology control is based on a fine-tuning of anisotropic, intermolecular solute–solute interactions that are attenuated by the solute–solvent interaction in organic solvents of different chemical structure. We discuss the role of light illumination in the self-assembly process as well as application of ultrasonic treatment as a way of mechanical tailoring of morphology. This approach paves the way toward the molecular-scale tailoring of structural properties of organic semiconducting materials for electronic and optoelectronic applications.



INTRODUCTION

Molecular self-assembly in the liquid phase is the means by which living things are created in Nature. Sometimes incredibly sophisticated, sometimes elegantly simple, biological systems have been evolving toward a variety of architectures that sustain versatile aspects of life through multitude of functionalities. The astonishing versatility of functionalities in Nature and efficiency of the processes provide an enormous encouragement for utilizing the same principles to create artificial, biomimetic devices. The vast majority of such objects are enabled by the noncovalent, intermolecular bonding mechanisms, such as metal ion-ligand coordination, hydrogen bonding, $\pi-\pi$ stacking, steric interactions, etc.¹ A $\pi-\pi$ interaction between discotic (disk-like) molecules is of particular interest for making biomimetic electronic and optoelectronic devices. While the interaction between their aromatic cores serves as a noncovalent bonding mechanism for molecular self-organization into complex matter,² stacks of discotic molecules provide one-dimensional, highly efficient channels for charge carrier transport.³ This class of materials paves the way toward making biomimetic optoelectronic materials and devices by combining the tools of synthetic and supramolecular chemistry for designing new materials with the knowledge of optical properties and electronic processes in more traditional organic semiconducting materials such as organic molecular crystals.⁴

The $\pi-\pi$ interactions between discotic molecules are typically viewed as electrostatic in nature. On the interatomic length scale, they are satisfactorily described by the Sanders and Hunter model² where the electrostatic potential energy between the positively

charged nuclei and a negative charge of electronic orbitals is minimized to deduce the optimal position of molecules in the stacks. On the longer, intermolecular length scale these can be viewed as interacting electric multipoles. Therefore, the $\pi-\pi$ interaction is expected to be anisotropic and the force field for long-range, attractive forces should decay in space according as multipoles ($\propto 1/r^3$ for dipoles, $\propto 1/r^4$ for quadruples, etc.). A number of previous studies on self-assembly of discotic molecules have focused on molecules with the cores of higher symmetry groups such as hexabenzocoronene (HBC; C_6),⁵ phthalocyanine (C_4),⁶ and triphenylene (C_3)⁷ that produced one-dimensional, fibrous geometries if the intermolecular association constants were large enough to sustain such growth. The self-assembly of molecules of lower symmetry such as the ones with the perylene diimide core (C_2) is expected to produce qualitatively different morphologies due to the anisotropy of their intermolecular interactions.

In solution-phase self-assembly, the solvent molecules modulate the intermolecular solute–solute interactions via solute–solvent and solvent–solvent interactions, yielding an additional degree of freedom for controlling the self-assembly process.⁸ Previous studies of solution-based self-assembly of molecules with the perylene diimide core focused on symmetrically substituted derivatives, precipitating the one-dimensional (“belt-like”) nanostructures from

Received: April 20, 2011

Revised: June 21, 2011

Published: June 29, 2011

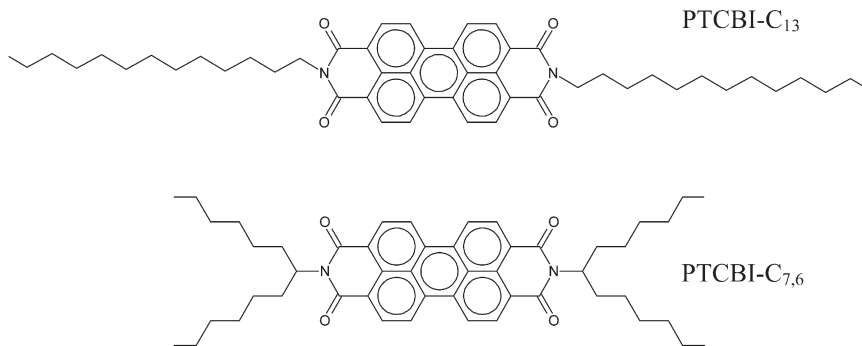


Figure 1. Molecular chemical structures of PTCBI-C₁₃ and PTCBI-C_{7,6} derivatives.

a mixture of poor and good solvents,^{9,10} or growing them from a single-phase solvent using graphene oxide as a seeding agent.¹¹ Self-assembly of asymmetrically substituted derivatives have resulted in richer morphologies.¹² In terms of potential applications, materials with the perylene diimide core are known to be efficient electron conductors (*n*-type semiconductors)¹³ that are complementary to more common, hole-conducting organic semiconductors. Both types of materials constitute the basis of low-power-consumption CMOS technology based on complementary inverters¹⁰ as well as enable electron donor–acceptor architectures in photovoltaic devices.¹⁴ The studies of electronic transport processes as well as optical properties^{11,15} of molecular aggregates based on molecules with PTCBI cores provide a complementary knowledge base for correlating molecular chemical structure with the structural properties of self-assembled materials and their functionality. Such materials are a convenient model system for fundamental studies as well as with prospects for practical applications.

In this paper, we exploit the role of anisotropy of intermolecular interactions of *N,N'*-ditridecylperylene-3,4,9,10-tetracarboxylic diimide in the process of solution phase self-assembly of such molecules into highly ordered structures of well-defined morphologies. The morphologies range from gel-type, fibrous phases to one-dimensional and two-dimensional ones. We discuss how a precise control over the morphologies can be exerted by a rational selection of the self-assembly solvent medium, as well as by varying processing conditions, such as temperature and illumination. The goal of this research is to explore available options for molecule-scale tailoring of structural properties and functionality of organic optoelectronic materials for photovoltaic applications. In the long run, we aim at developing a rationale for molecular-scale tailoring of structural properties of organic semiconductors that are created in the process of hierarchical self-organization for a broad range of specific, predetermined functionalities.

MATERIALS AND METHODS

Two commercially available (Sigma-Aldrich) perylene diimide derivatives, *N,N'*-ditridecylperylene-3,4,9,10-tetracarboxylic diimide and *N,N'*-bis(1-hexylheptyl)-perylene-3,4,9,10-bis-(dicarboximide), denoted as PTCBI-C₁₃ and PTCBI-C_{7,6}, respectively, were used in this study. Their molecular chemical structures are shown in Figure 1. Both materials were used as purchased (98% purity). However, the self-assembled materials are expected to be purer. While being similar to precipitation from a mixture of good and poor solvents, an approach that exploits different solubility of impurities for materials purification, the solution-phase self-assembly specifically profits from a selectivity of intermolecular interactions based on chemical

compatibility, complementarity, and so on, of noncovalent bonding groups.

These two perylene diimide derivatives differ by the chemical structure of their side chains. The nodes in the highest occupied molecular orbital (HOMO) and the lowest unoccupied molecular orbital (LUMO) at the imide nitrogens of PTCBI core decouple the π -conjugated system of the core from the electronic orbitals of side chains.^{15,16} If the aggregation behavior of PTCBI molecules depends on the nature of side chains, spectroscopic features of the aggregates absorption can sometimes be used to deduce the relative position of molecular cores in the aggregates (H-type vs J-type) and can, therefore, serve as an in situ tool for monitoring the aggregation process.¹⁷ It has been previously found that the linear and branched side chains of PTCBI derivatives lead to a different solubility of these materials in common organic solvents.⁹ While the former material tends to self-assemble into “belt-like” structures, the latter one is soluble, presumably due to a steric hindrance between the branched side chains. Similarly, steric hindrance between the branched side chains of a certain length reduces the association constants in self-assembly of HBC derivatives, while the longer chains moderately facilitate the association due to van der Waals interactions between them.⁵ The extinction coefficient of a PTCBI-C_{7,6}, soluble materials due to its branched side chains, measured in a dilute solution (as discussed in the Supporting Information, Figure S1) can be used, therefore, as a reference of PTCBI monomer absorption.

We used the UV–vis-NIR absorption spectroscopy, steady state photoluminescence spectroscopy, optical microscopy, scanning electron microscopy (SEM), and atomic force microscopy (AFM) for characterizing the optical and morphological properties of PTCBI solutions and the self-assembled structures. The UV–vis-NIR absorption spectroscopy was done using the CARY 500 spectrophotometer and quartz cuvettes of different thicknesses, ranging from 100 μ m to 10 mm. The temperature-dependent UV–vis-NIR absorption measurements were done combining the aforementioned instrument with the INSTECH 200 controller and a hotstage. A Photon Technology International (PTI) fluorimeter in a custom configuration was used for the steady state photoluminescence spectroscopy. The Hitachi 4500 scanning electron microscope (Swagelok Center for Surface Analysis of Materials, CWRU) and JEOL JSM 6320F scanning electron microscope (MRSEC, University of Massachusetts) were used for SEM measurements with an electron accelerating voltage of 5 kV. The ultrathin gold films were sputtered onto the samples prior to the SEM imaging to improve the image contrast. The MFP-3D atomic force microscope (Asylum Research) in an ac (noncontact) mode was used for the AFM imaging. A spring constant of silicon tips was 20–80 N/m and a resonant frequency of 312–342 kHz for different tips. Comparing

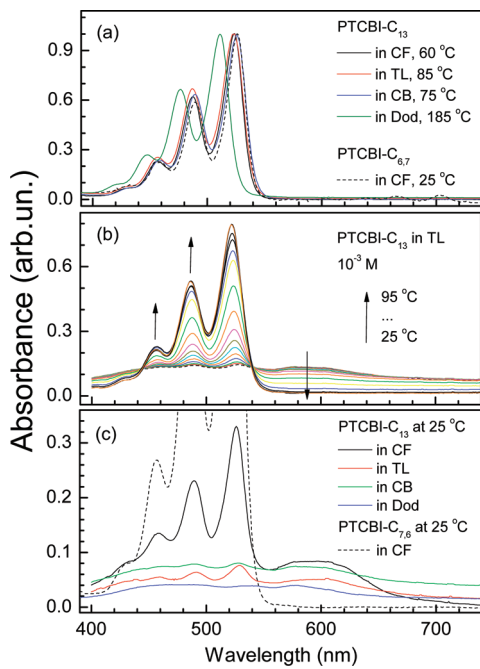


Figure 2. Spectral dependence of PTCBI-C₁₃ absorbance (a) in a monomer state in various solvents at high temperatures, (b) on heating in TL during aggregates transformation, and (c) at room temperature in the aggregated state in various solvents. The absorption spectrum of soluble PTCBI-C_{7,6} in CF is shown for comparison.

the results of AFM imaging for pristine and gold-covered samples (not shown), the gold layer typically slightly smoothes the finer surface features. However, the size of these features was well below the SEM resolution.

RESULTS AND DISCUSSION

Powdered PTCBI-C₁₃ was dispersed in chloroform (CF), toluene (TL), chlorobenzene (CB), or dodecane (Dod). The solubility of PTCBI-C₁₃ is poor in these solvents at room temperature and it improves significantly upon heating. Intermolecular association/dissociation leads to changes in the electronic structure of molecules and aggregates. Therefore, UV-vis-NIR absorption spectroscopy can be used as an *in situ* monitoring tool for such processes. Figure 2a compares the absorbance of PTCBI-C₁₃ (5×10^{-4} M) in CF at 60 °C, in TL at 85 °C, in CB at 75 °C, and in Dod at 185 °C with the absorbance of PTCBI-C_{7,6} monomers in CF at 25 °C. The peaks at 526, 488, and 457 nm were previously attributed to S₀ → S₁ electronic transition and its vibronic overtones in the PTCBI-C_{7,6} monomers, respectively.¹⁸ The spectra of PTCBI-C₁₃ in all solvents, except in Dod, closely resemble the spectrum of PTCBI-C_{7,6} in CF. While the spectrum in Dod is characterized by the same magnitudes of the peaks, the shift of the spectra arises due to larger relative solvent polarities of CF (0.259), CB (0.188) and TL (0.099) as compared to Dod (0.012).¹⁹ A close match of the spectra shows that all solutions are in nearly a monomer state at the indicated temperatures. This was further supported by the fact that the spectra remained unchanged upon further heating of solutions. All the PTCBI-C₁₃ solutions were therefore heated up to the indicated temperatures as the first step in fabricating the self-assembled nanostructures where all the solutions were assumed to be in monomer state. We would like to note that the range of temperatures where a complete dissociation of aggregates occurs is very broad for different solvents. For any given solvent, the

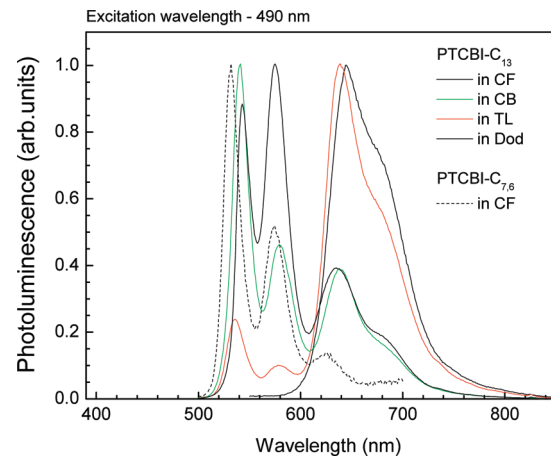


Figure 3. Spectral dependence of PTCBI-C₁₃ photoluminescence in various solvents and of PTCBI-C_{7,6} in CF at room temperature. The spectra were normalized to their respective maxima.

temperature of dissociation is typically about 10–20° below the solvent boiling point.

Subsequent cooling of monomer solutions leads to a strong aggregation of PTCBI-C₁₃ in all studied solvents. Figure 2c shows the absorbance spectra of PTCBI-C₁₃ at room temperature after the self-assembly process has been completed. The absorbance of PTCBI-C_{7,6} monomers is also shown for comparison. Comparing to the monomer absorption, there are two distinct features in the absorption spectra of aggregates. First, aggregation leads to formation of absorption band between 550 and 650 nm. Such wavelength range is a signature of efficient interaction of transition dipole moments of PTCBI cores in J-type (head-to-tail) geometry in the aggregates.¹⁷ We would like to note that all solutions, except of CF, contained aggregates and were otherwise colorless and clear once the self-assembly process was completed. While the CF solution also contained an aggregate, it retained its orange color at room temperature. The color was not as intense as at high temperature however. This is the evidence of a slight solubility of PTCBI-C₁₃ in CF and its absorption spectrum is therefore a combination of the aggregate and monomer absorption. Second, the oscillator strength of the electronic transitions gradually decreases as the aggregation proceeds. Figure 2b shows the temperature dependence of PTCBI-C₁₃ absorbance in TL upon heating from 25 to 95 °C. A gradual transformation of the absorption spectra from the aggregated state to a monomer one takes place. The well-defined isosbestic points in the spectra show that it is a two-phase solution,²⁰ consisting of large-size aggregates and monomers. The features at the wavelengths above 660 nm are probably due to light scattering by the submicrometer size aggregates that has not been accounted for.

Figure 3 shows the photoluminescence spectra of the aggregated PTCBI-C₁₃ in different solvents as well as of PTCBI-C_{7,6} monomers in CF at 25 °C. The spectra in CF and CB resemble the monomer photoluminescence; however, they also contain an additional shoulder at 685 nm. In a series of CF, TL, and Dod, the photoluminescence spectra gradually change and the features at 640 and 685 nm dominate. In dodecane, the monomer photoluminescence is completely diminished and the spectrum is entirely dominated by the lower energy peaks that resulted from aggregation. Note that the 530 nm peak in CF solution is strongly attenuated by the reabsorption.

Figure 4 shows the optical microscopy images of PTCBI-C₁₃ nanostructures that were self-assembled in CF (a), CB (b,e), Dod

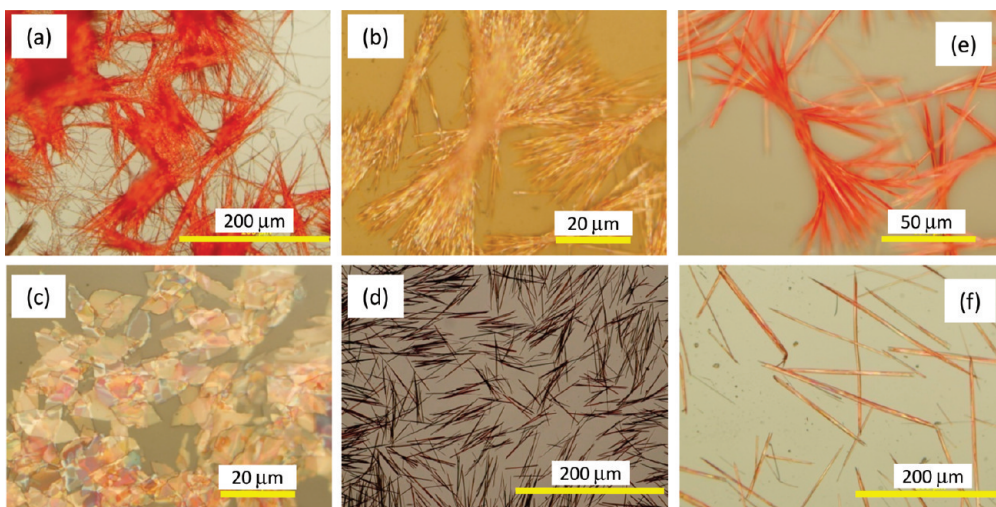


Figure 4. Optical microscopy images of PTCBI-C₁₃ aggregates that were self-assembled in (a) CF, (b) CB, (c) Dod, and (d) TL under illumination and in (e) CB and (f) TL in the dark. Note the different length scales of images.

(c), or TL (d,f) according to the procedure that included a heating of solutions to a monomer state and their subsequent cooling down to the room temperature. Despite a similarity of absorbance spectra of PTCBI-C₁₃ aggregates in different solvents, which reflects similar molecular packing, the aggregates possess distinct, qualitatively different macroscopic morphologies. In CF, the molecules form a fibrous, gel-type morphology. In CB, the fibrous structures are assembled into bundles. In TL, the molecules are assembled into individual “belt-like” structures. The latter morphology is similar to the one previously obtained by a CF/methanol precipitation.⁹ It has been previously reported that the one-dimensional geometry of molecules with PTCBI core results from a high growth rate due to $\pi-\pi$ interactions.^{9,10} The $\pi-\pi$ stacking along the belt direction has been further confirmed by the XRD measurements and this crystallographic orientation was assigned as *a-a*.¹⁰ While the $\pi-\pi$ interaction between the aromatic cores is the dominating association mechanism for discotic molecules, the effect of long branched alkyl side chains can not be neglected.²¹ While all the structures in CF, CB, and TL consist of fibrous (one-dimensional) structural units, the transverse size of fibrils becomes bigger in the respective series of solvents. This suggests that these solvents primarily attenuate the growth rates along the two transverse directions. The morphology in Dod is a two-dimensional one. The Dod molecules effectively screen the $\pi-\pi$ interactions preventing one-dimensional growth along *a-a* orientation.

The effect of illumination on the resulting morphologies can be seen by comparing the self-assembled structures that were fabricated under illumination by the fluorescent laboratory lights (Figure 4b in CB and Figure 4d in TL) and in the dark (Figure 4e in CB and Figure 4f in TL). The morphologies that were fabricated in the dark, while qualitatively similar to the ones that were fabricated under illumination, are characterized by the features of a larger size. We therefore conclude that the specified light illumination reduces the size of features in CB and TL. There was no noticeable effect of the indicated illumination conditions on the morphologies in CF and Dod. All the discussed self-assembly processes were conducted under the identical illumination conditions, if otherwise is not indicated, since such conditions produced more favorable morphologies for practical applications of interest. The pronounced effect of illumination on

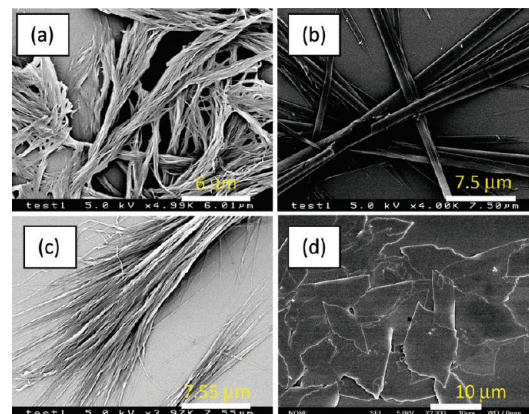


Figure 5. SEM images of PTCBI-C₁₃ aggregates deposited from (a) CF, (b) TL, (c) CB, and (d) Dod.

the resulting morphologies also shows that the UV-vis-NIR spectroscopy can not be regarded as a completely nonperturbing characterization tool.

Finer morphological features of the PTCBI-C₁₃ structures self-assembled in different solvents can be seen in SEM images (Figure 5). A gel-like morphology in CF (Figure 5a) is a dilute cross-linked network. The material aggregates into a single piece in CF, while the micrometer-size aggregates in TL, CB, and TL can be uniformly dispersed. The fibrous units form bundles in CB (Figure 5c). Figure 7b shows the same material where a central part of the bundle is shown. The bundles look rather like an association of independent fibrils than the fibrils that grow from a single nucleation center. In Dod, the material forms “flakes” with the two in-plane growth direction being nearly equivalent. The edges of the flakes are not as sharp as in TL nanobelts. This further indicated that there is no strong asymmetry between the two in-plane growth rates in Dod.

The geometry and molecular packing in the self-assembled structures were further studied by AFM imaging. Figure 6 shows the PTCBI-C₁₃ nanobelts deposited from TL (Figure 6a, 2D height profile) and microflakes deposited from Dod (Figure 6b, amplitude profile). These images show the growth terraces on

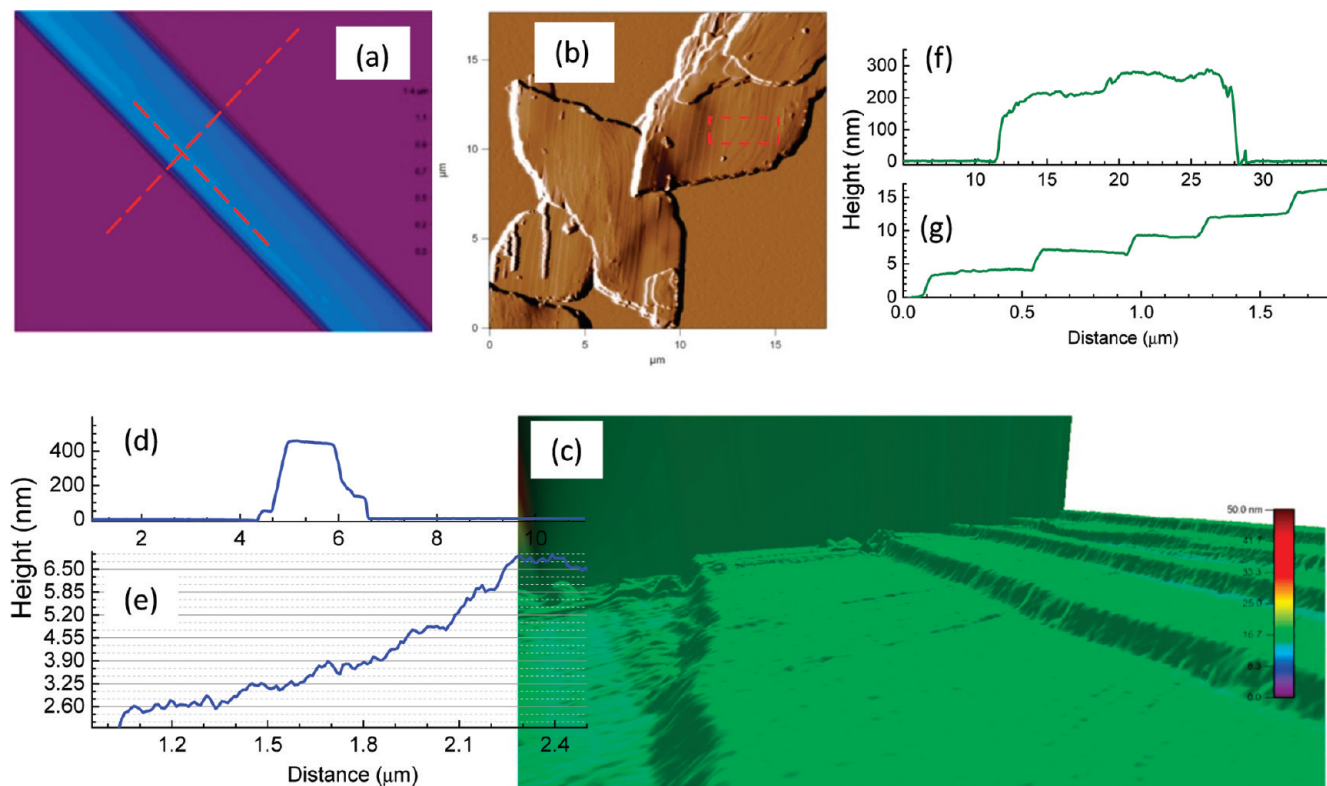


Figure 6. AFM images of PTCBI-C₁₃ aggregates deposited from TL (a, 3D height profile) and Dod (b, amplitude profile; c, 3D height profile), as well as their transverse and longitudinal cross sections in TL, (d) and (e), respectively and in Dod, (f) and (g), respectively.

the surfaces of both types of nanostructures. As expected, the uncompleted terraces propagate along the long axis of the nanobelts, consistent with the fastest growth rate along *a-a* direction. The edges of the belts are very sharp that again points to the high anisotropy of growth rates, as well as evidences the highly ordered molecular packing within the nanobelts. In the microflakes, the terraces propagate across the entire flake along some preferred direction. This indicates that each flake is a single crystal with a clear molecular packing anisotropy with two comparable in-plane growth rates. Figure 6d and f show cross sections of the nanobelt along the transverse direction and of the flake, respectively. The given nanobelt is about 550 nm tall and roughly 1.5 μm wide. While the particular set of sizes is strongly dependent on solution concentration that has been used during the self-assembly process (10^{-3} M in this case),²² the ratio between the length, width, and height of the nanobelt, 20000:1500:550, can be used as an estimate of the growth rates along the respective directions. While there is no well-defined in-plane size quantization in the microflake geometry, the typical range of sizes is 5–15 μm for a solution of 10^{-3} M. The height of the flakes is about 200–300 nm and some finer, 100 nm tall layers can be resolved. The ratio between the flake height and the in-plane sizes suggests that the growth rate along the flake thickness is about 500 times slower than in the other two directions.

Figure 6c shows the 3D topography of the flake (section of Figure 6b enclosed in the dashed rectangle). Its cross-section across the steps is given in Figure 6g. There are a number of well-quantized steps and the average size of each step is 3.2 nm. Such size is similar to 3.1 nm, which is the size of PTCBI-C₁₂ molecules (note shorter side chain) along its extended axis. We therefore conclude that the slowest growth direction in Dod is *c-c* where the molecules are

stacked due to van der Waals interactions between the alkyl side chains. The growth rates along *a-a* ($\pi-\pi$ stacking) and *b-b* directions are therefore comparable in Dod. The longitudinal cross-section of the nanobelt grown in TL (Figure 6e) contains less pronounced steps with the smallest quantized features of 0.65 nm. This value is close to the size of the PTCBI core along its short axis (0.8 nm) that is tilted. While surprising, we conclude that the slowest growth direction in TL is a *b-b* one. The relatively smooth features in the longitudinal cross-section of the nanobelts are consistent with this model. While it is more difficult to measure the smaller size features on the top of a flexible, 550 nm tall belt in general, the edges of terraces are also composed of alkyl side chains in this case. The chains are disordered and, therefore, no sharp steps would be expected. In the case of flakes, the alkyl side chains form the top surfaces of the terraces and the edges are created by the sides of rigid PTCBI cores, and therefore more well-defined.

It has been previously shown that the fastest growth direction of molecules with a PTCBI core and linear alkyl side chains,^{9,10} as well as of other discotic molecules in aromatic solvents, is the $\pi-\pi$ stacking. We found that Dod, a nonaromatic solvent with a small relative solvent polarity and zero dipole moment effectively screens the growth along the $\pi-\pi$ stacking direction and prevents the one-dimensional growth. This complements the fact that aromatic solvents, opposite to expectations, do not screen the interactions between aromatic cores along the $\pi-\pi$ stacking direction. In particular for HBC and PAM derivatives, it has been observed that aromatic solvents lead to stronger association of molecules due to aromatic core interactions.²³ However, the PTCBI-C₁₂ molecules still form the fibrous structures in hexane.⁹ We therefore conclude that the role of solvent molecules with a zero dipole moment is to limit the

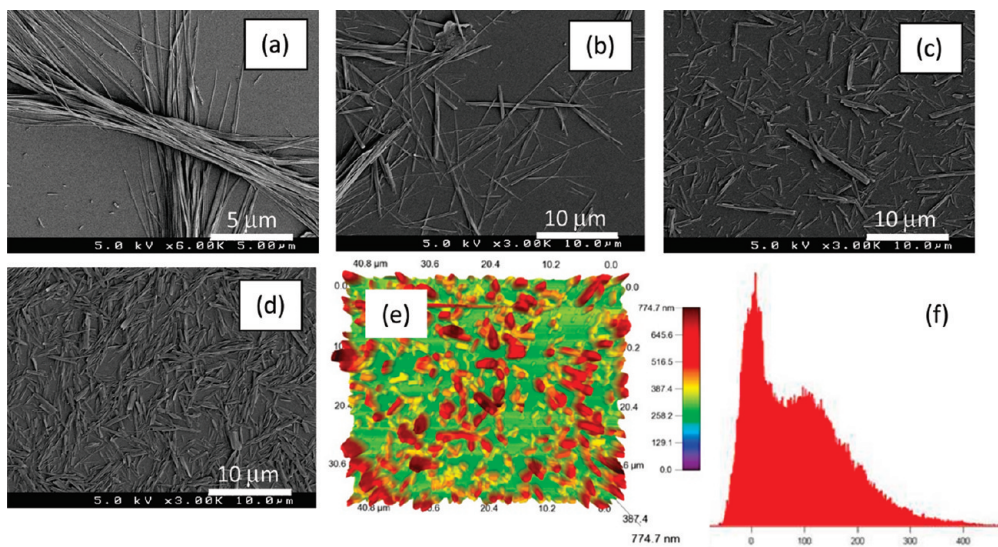


Figure 7. SEM images of PTCBI-C₁₃ aggregates deposited from CB solution before ultrasonic treatment (a) and after the treatment for (b) 1, (c) 5, and (d) 15 min; (e) AFM topography of the material after 15 min of treatment and (f) its height histogram.

available closest distance that the two π -conjugated cores can approach each other, therefore, reducing the interaction energy between them according to the multipoles interaction model. While the difference between the other three polar solvents for the growth rates along the $\pi-\pi$ stacking direction can not be resolved from our measurements, these solvents noticeably change the growth rates along the transverse directions of the fibrous structures. The growth rates in CF are most asymmetric, being fastest along the $\pi-\pi$ stacking direction, as evidenced from the narrowest fibrous structures. The fibrils are further randomly organized into a gel-type structure. In CB, while the growth along *a-a* direction is still the fastest one, the growth rates along *b-b* and *c-c* directions are more comparable and therefore the fibrils are thicker. This trend continues in TL.

Considering the discussed mechanism of intermolecular interactions, it is not surprising that the illumination has such a strong effect on the aggregation behavior. The shapes of HOMO and LUMO orbitals and, therefore, the $\pi-\pi$ intermolecular interactions are different for the molecules in the ground and excited states, respectively.¹⁶ Surprisingly, qualitatively similar morphologies with larger size features in the dark were found. This suggests that the illumination primarily affects the growth rates in the transverse directions. Presumably, the intermolecular interactions between the photoexcited molecules become weaker under the illumination. The fact that some solvents affect the self-assembly of PTCBI-C₁₃ molecules in the photoexcited state stronger is in good agreement with the differing spectral features of photoluminescence of this material in those solvents (Figure 3).

Highly ordered, nanostructured organic materials are of potential interest for electronic and optoelectronic applications. A substrate-independent molecular packing, high degree of structural order that frequently leads to large mobilities as well as the absence of grain boundaries that are detrimental for operation are key features for efficient operation of the thin-film field-effect transistors. Also, the small size and flexibility of the self-assembled materials are attractive properties for their practical applications. The nanobelts, similar to the ones that were self-assembled in TL here, have been already utilized in field-effect transistors and resulted in satisfactory performance.¹⁰ Application of such materials in the photovoltaic

devices imposes additional requirements on the materials morphology. In particular, for their application as scaffolds of bulk heterojunction blends, the nanofiber diameter and length should be comparable to the exciton diffusion length in the transverse direction and to the inverse absorption coefficient in the longitudinal one, on the order of 10 and 100 nm, respectively. The anisotropy of intermolecular interactions due to which the nanostructures of various shapes and geometries are produced should also lead to anisotropic mechanical properties of the self-assembled nanostructures. We therefore exploited the approach of mechanical treatment of bundles self-assembled in CB by ultrasonic treatment in an attempt to reduce the sizes of the aggregate structures.

Figure 7 shows the SEM images of the bundles that were processed from CB prior to ultrasonic treatment (a) and after 1 (b), 5 (c), and 15 min (d) of treatment at 42 kHz. As it is evident from the figure, sonication separates the bundles along the long axis first, making the individual nanobelts, and then breaks the belts perpendicular to their long axes. The longer sonication times (15 min) lead to a more uniform size distribution. Figures 7e and 7f show the AFM image of the resulting aggregates after 15 min of sonication and its histogram, respectively. The average length of the pieces is about 2 μ m. We believe that this size is related to the frequency of an ultrasonic wave (42 kHz) used to treat the bundles and to the typical size of bubbles during the cavitation process. It would be expected that the higher frequencies that lead to a smaller size of bubbles would further reduce the length of the nanobelts. This procedure seems to split the bundles, however, not to change the width of the individual belts. The average height of the belts determined from the histogram is 100 nm. While the final sizes of the structures are closer to those desired for practical applications, they still need to be further reduced.

CONCLUSIONS

We studied a self-assembly of the perylene diimide derivative, *N,N'*-ditridecylperylene-3,4,9,10-tetracarboxylic diimide, into structures of various morphologies in organic solvents. The approach for producing well-defined morphologies is based on the intermolecular interactions between the molecules of a

perylene diimide derivative, such as $\pi-\pi$ interaction between the aromatic cores, and on a temperature control of solubility. The process was found to be strongly dependent on such parameters as temperature, chemical structure of solvent molecules, concentration of solutions, and illumination conditions. Precise control of the process conditions allows for making the very well-defined morphologies in the self-assembly process which produced one-dimensional (belt-like) structures with various transverse sizes in a series of TL, CB, and CF or two-dimensional morphology in Dod. We suggest that the shape anisotropy is a result of anisotropic intermolecular interactions that are further attenuated by the medium in which the self-assembly process takes place, namely by the organic solvent. We speculate that the effect of light illumination on self-assembly is to change the geometry of electronic orbitals upon the electron photoexcitation from HOMO to LUMO and, therefore, to affect the intermolecular interaction. Ultrasonic treatment of aggregates was found to be an effective approach for reducing the sizes of aggregates. Higher frequencies of ultrasonic treatment, more dilute solutions, and intense light illuminations are expected to produce the structures with smaller sizes. Overall, the approach of a solution-phase, molecular self-assembly has a potential to produce extremely pure, highly ordered organic optoelectronic materials with the structural properties that can be tailored for specific functionalities and lead to a cost-effective device fabrication.

■ ASSOCIATED CONTENT

S Supporting Information. Concentration-dependent UV-vis-NIR absorption spectra of PTCBI-C_{7,6} in chloroform. This material is available free of charge via the Internet at <http://pubs.acs.org>.

■ AUTHOR INFORMATION

Corresponding Author

*Tel.: 413-577-0902. E-mail: duzhko@mail.pse.umass.edu.

■ ACKNOWLEDGMENT

This work was partially supported by the Polymer-Based Materials for Harvesting Solar Energy, an Energy Frontier Research Center funded by the U.S. Department of Energy, Office of Science, Office of Basic Energy Sciences under Award Number DE-SC0001087.

■ REFERENCES

- (1) Lehn, J. M. *Science* **2002**, *295*, 2400–2403.
- (2) Hunter, C. A.; Sanders, K. M. *J. Am. Chem. Soc.* **1990**, *112*, 5525–5534.
- (3) Adam, D.; Schuhmacher, R.; Simmerer, J.; Haussling, L.; Siemsmeyer, K.; Etzbach, K. H.; Ringsdorf, H.; Haarer, D. *Nature* **1994**, *371*, 141–143.
- (4) Pope, M.; Swenberg, C. E. *Electronic Processes in Organic Crystals and Polymers*; Oxford University Press: New York, 1999.
- (5) Kastler, M.; Pisula, W.; Wasserfallen, D.; Pakula, T.; Müllen, K. *J. Am. Chem. Soc.* **2005**, *127*, 4286–4296.
- (6) Duzhko, V.; Singer, K. D. *J. Phys. Chem. C* **2007**, *111*, 27–31.
- (7) Koshkakaryan, G.; Jiang, P.; Altoe, V.; Cao, D.; Klivansky, L. M.; Zhang, Y.; Chung, S.; Katan, A.; Martin, F.; Salmeron, M.; Ma, B. W.; Aloni, S.; Liu, Y. *Chem. Commun.* **2010**, *46*, 8579–8581.
- (8) Duzhko, V.; Shi, H.; Semyonov, A. N.; Twieg, R. J.; Singer, K. D. *Langmuir* **2006**, *22*, 7947–7951.

- (9) Balakrishnan, K.; Datar, A.; Naddo, T.; Huang, J. L.; Oitker, R.; Yen, M.; Zhao, J. C.; Zang, L. *J. Am. Chem. Soc.* **2006**, *128*, 7390–7398.
- (10) Briseno, A. L.; Mannsfeld, S. C. B.; Reese, C.; Hancock, J. M.; Xiong, Y.; Jenekhe, S. A.; Bao, Z.; Xia, Y. *Nano Lett.* **2007**, *7*, 2847–2853.
- (11) Bao, Q.; Goh, B. M.; Yan, B.; Yu, T.; Shen, Z.; Loh, K. P. *Adv. Mater.* **2010**, *22*, 3661–3666.
- (12) Yao, P. J.; Yang, X.; Xu, X. H.; Lu, Y. Q.; Ji, H. F.; Dai, S. *J. Mater. Sci.* **2011**, *46*, 188–195.
- (13) Duzhko, V.; Aqad, E.; Imam, M. R.; Peterca, M.; Percec, V.; Singer, K. D. *Appl. Phys. Lett.* **2008**, *92*, 113312.
- (14) Schmidt-Mende, L.; Fechtenkötter, A.; Müllen, K.; Moens, E.; Friend, R. H.; MacKenzie, J. D. *Science* **2001**, *293*, 1119–1122.
- (15) Chaudhuri, D.; Li, D.; Che, Y.; Shafrazi, E.; Gerton, J. M.; Zang, L.; Lupton, J. M. *Nano Lett.* **2011**, *11*, 488–492.
- (16) Würthner, F. *Chem. Commun.* **2004**, 1564–1579.
- (17) Kasha, M.; Rawls, H. R.; El-Bayoumi, M. A. *Pure Appl. Chem.* **1965**, *11*, 371–392.
- (18) Langhals, H.; Karolin, J.; Johansson, L. B. A. *J. Chem. Soc., Faraday Trans.* **1998**, *94*, 2919–2922.
- (19) Reichardt, C. *Solvents and Solvents Effects in Organic Chemistry*, 3rd ed.; Wiley-VCH: Weinheim, 2003; *the value of *n*-heptane is given, and the relative solvent polarity of dodecane was assumed to be similar.
- (20) See, for example, Moore, J. W.; Pearson, R. G. *Kinetics and Mechanism*, 3rd ed.; John Wiley and Sons: New York, 1981; p 49.
- (21) Kastler, M.; Pisula, W.; Wasserfallen, D.; Pakula, T.; Müllen, K. *J. Am. Chem. Soc.* **2005**, *127*, 4286–4296.
- (22) We observed that the morphology of self-assembled structures did not change qualitatively, however the sizes of all the features increase if the self-assembly is performed in more concentrated solutions. We believe that the growth stops when the molecules deplete the solution. The detailed concentration-dependent studies were not performed, however.
- (23) Tobe, Y.; Utsumi, N.; Kawabata, K.; Nagano, A.; Adachi, K.; Araki, S.; Sonoda, M.; Hirose, K.; Naemura, K. *J. Am. Chem. Soc.* **2002**, *124*, 5330–5364.